# Magnetic properties and structure of Gd-implanted L10 FePt thin films

**J. Hintermayr, N. Y. Safonova, Aladin Baldur Bernd Ullrich, Manfred Albrecht**

**Angaben zur Veröffentlichung / Publication details:**

Hintermayr, J., N. Y. Safonova, Aladin Baldur Bernd Ullrich, and Manfred Albrecht. 2019. "Magnetic properties and structure of Gd-implanted L10 FePt thin films." *AIP Advances* 9 (5): 055020. https://doi.org/10.1063/1.5097350.

# Magnetic properties and structure of Gd-implanted $L1_0$ FePt thin films

Cite as: AIP Advances **9**, 055020 (2019); https://doi.org/10.1063/1.5097350
Submitted: 25 March 2019 . Accepted: 13 May 2019 . Published Online: 23 May 2019

J. Hintermayr, N. Y. Safonova, A. Ullrich, and M. Albrecht

# Magnetic properties and structure of Gd-implanted $L1_0$ FePt thin films

Cite as: AIP Advances 9, 055020 (2019); doi: 10.1063/1.5097350
Submitted: 25 March 2019 • Accepted: 13 May 2019 •
Published Online: 23 May 2019



J. Hintermayr,[a] N. Y. Safonova, A. Ullrich, and M. Albrecht

## AFFILIATIONS

Institut für Physik, Universität Augsburg, D-86159 Augsburg, Germany

[a]E-mail: julian.hintermayr@student.uni-augsburg.de

## ABSTRACT

In this study, we have investigated the effect of Gd implantation on composition, chemical order, and magnetic properties of 20 nm thick $L1_0$ ordered FePt thin films. We show that upon Gd implantation at 30 keV even a small amount of 1 at. % is sufficient to destroy the $L1_0$ order, resulting in a soft magnetic $A1$ FePt alloy, with the exception of a thin $L1_0$ ordered layer located at the film/substrate interface. Additionally, a strong resputter effect is observed which results in a large decrease in film thickness as well as to a reduction in Fe content in the FePt alloy. Post-annealing of samples in Ar atmosphere did not result in a restoration of the $L1_0$ order, but leads to a transformation to pure Pt and $Fe_2O_3$, facilitated by the presence of a high density of vacancies induced by the implantation process.



## I. INTRODUCTION

Chemically ordered $L1_0$ FePt alloy thin films, comprising of equal amounts of Fe and Pt, can exhibit large perpendicular magnetic anisotropy (PMA) of up to 70 Merg/cm$^3$.[1–3] Recently, these films have been implemented as storage material for applications in heat-assisted magnetic recording (HAMR), which is expected to further extend the areal density towards 3-4 Tb/inch$^2$.[4–8] While high PMA is needed for thermal stability of today's hard disk drives, it poses a challenge to magnetic writing heads, as heat assistance is generally required in order to reverse the magnetization direction.[8] Great interest therefore lies in the addition of third elements to the system, allowing for fine tuning of certain properties of the FePt alloy such as Curie temperature, saturation magnetization and PMA, as well as lowering the ordering temperature during post-annealing of chemically disordered FePt films.[9–16] In particular, the inclusion of rare earth elements can provide further functionalities.[17] For example, the addition of a heavy rare earth element should result in a reduction of the net magnetization due to the expectation of strong antiferromagnetic coupling between the magnetic moments of Fe and heavy rare earth element such as Gd.[18] Furthermore, it has been shown that the magnetization dynamics in ferrimagnetic GdFe stimulated by femtosecond laser pulses can offer an intriguing pathway for overcoming the material constraints of high magnetic anisotropy. In this regard, toggle switching in GdFe alloys, in which the magnetization switches back and forth after subsequent ultra short laser pulses, has been discovered.[18–21]

In this study, we have implanted Gd ions as third element to $L1_0$ ordered FePt thin films and investigated its impact on the structural and magnetic properties.

## II. METHODS

Crystal structures were analyzed by means of x-ray diffractometry (XRD). To characterize chemical compositions and film thicknesses, Rutherford backscattering spectrometry (RBS) was conducted with 5 MeV $He^{2+}$ ions. The Gd implantation was realized using an Eaton NV-3204 medium current implantation system. Simulations of the ion implantation process were performed utilizing the SRIM/TRIM software package.[22] A superconducting quantum interference device - vibrating sample magnetometer (SQUID-VSM) was used to measure the magnetic properties. Surface images were recorded using an atomic force microscope (AFM). Based on this data, the root mean square surface roughness $R_q$ was calculated. Scanning electron microscopy (SEM) images were taken at 10 kV probe energy and 100 pA probe current. Auger electron spectroscopy (AES) was performed at an Omicron NanoSAM system operating at 5 kV probe energy with 3 nA probe current. The hemispherical analyzer was operated in constant retard ratio mode.

## III. RESULTS AND DISCUSSION

$Fe_{52}Pt_{48}$ thin films with a thickness of 20 nm were prepared at 800 °C on single crystalline MgO(001) substrates by dc magnetron sputtering using an Ar pressure of 5 μbar. In order to be able to make a statement about the degree of chemical $L1_0$ ordering in the sample, an out-of-plane XRD $\theta/2\theta$-scan was carried out. As revealed in Fig. 1a, single crystalline films with $L1_0$ order and (002) orientation were obtained under these deposition conditions. Based on the ratio of the integrated intensities of the FePt(001) and FePt(002)

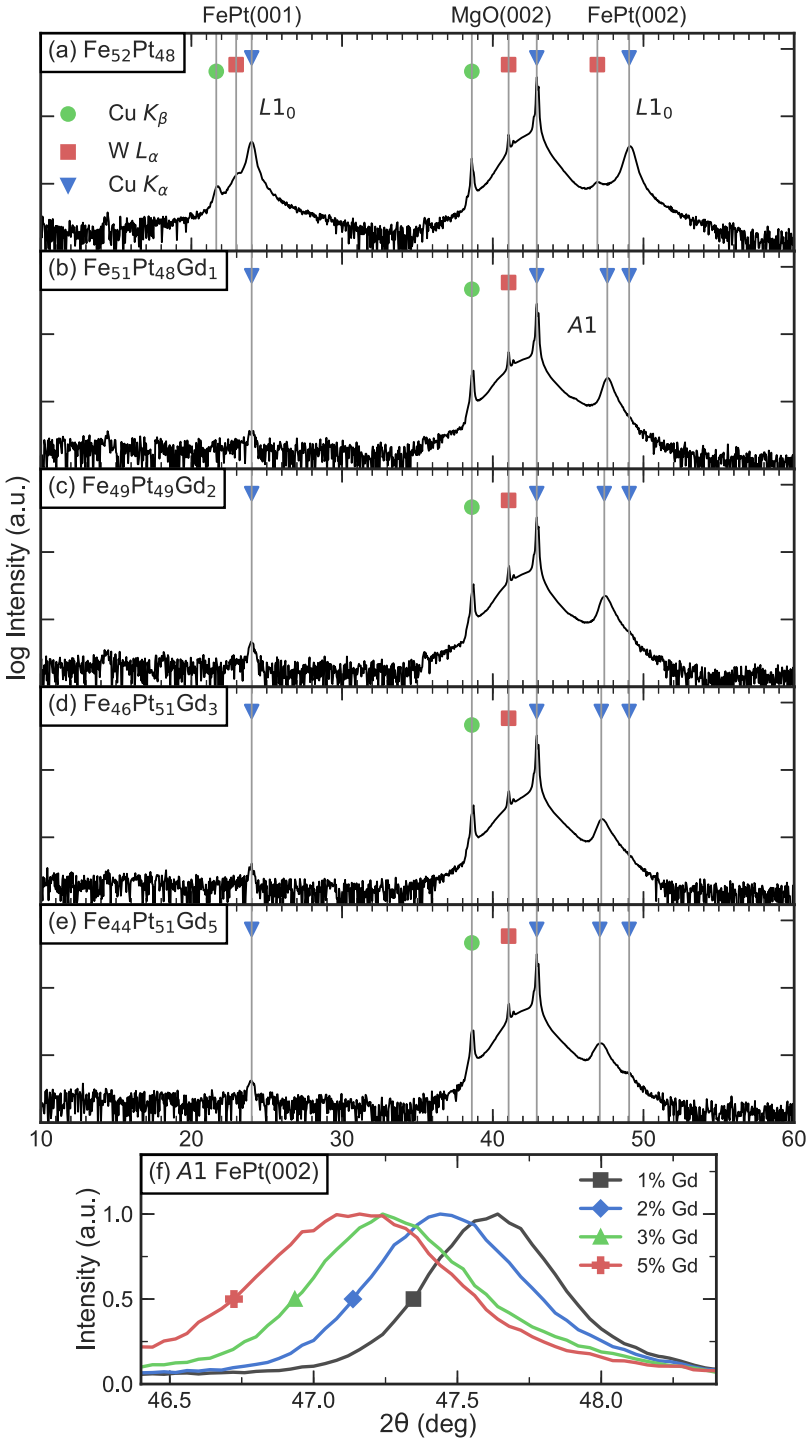


**FIG. 1**. XRD $\theta/2\theta$-scans of (a) as-prepared $L1_0$ FePt and (b-e) Gd-implanted FePt. (f) XRD $\theta/2\theta$-scan of Gd-implanted FePt films around the (002) peak position.

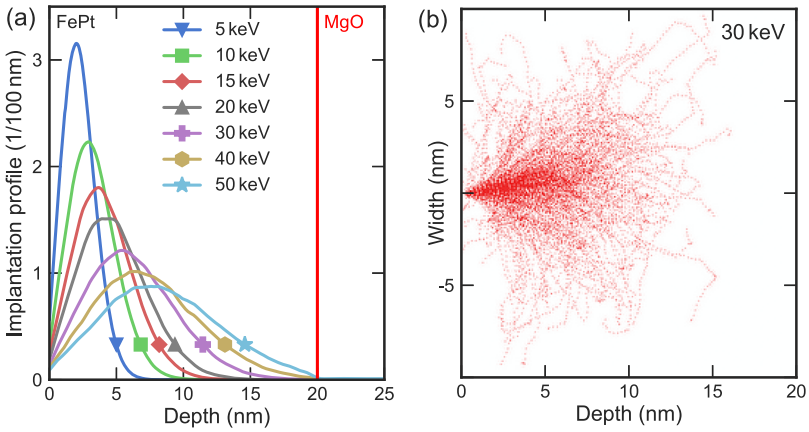


**FIG. 2**. (a) Implantation profile as a function of depth for Gd ions in FePt at different ion energies. (b) Gd ion trajectories in FePt at an energy of 30 keV. Simulations were carried out by TRIM.

diffraction peaks the order parameter was determined to be 0.77, taking into account structure factor, absorption factor, polarization and Lorentz factor as well as the thermal displacement factor, as described by B. W. Roberts.[23] An experimental Debye-Waller factor of 0.14 Å, reported for FePt,[24] was used to calculate the thermal displacement factor. Its magnetic properties were characterized by measuring in-plane and out-of-plane *M-H* hysteresis loops at 300 K. The corresponding loops are shown in Fig. 4a, revealing a clear out-of-plane easy axis of magnetization. It was not possible to saturate the sample in the magnetically hard in-plane direction due to the high magnetocrystalline anisotropy constant of the $L1_0$ phase, which was estimated to be in the range of 40 Merg/cm$^3$. Please note that we have measured a rather high saturation magnetization of the prepared $L1_0$ FePt film, which is about 20% larger than typically reported in the literature.[25] The reason for this discrepancy is still not clear but the conclusions drawn are not affected by this. The surface roughness $R_q$ of the sample was calculated to be 1.7 nm based on AFM measurements.

These film samples were further used for Gd implantation studies. Before Gd implantation, the correct fluence of Gd atoms per cm$^2$ as well as the ion energy for the process had to be determined. Therefore, numerical TRIM simulations were conducted, simulating the behaviour of accelerated Gd ions in 20 nm thick FePt films. Various runs at different ion energies, ranging from 10–50 keV, were simulated. The results are shown in Fig. 2a. For increasing energies, the maximum in Gd concentration shifts towards the substrate and the curves flatten out. A desirable distribution has its maximum at a sufficient depth below the surface, without penetrating into the MgO substrate, as the interface between the FePt film and the substrate should remain intact. The Gd distribution corresponding to an ion energy of 30 keV satisfies both requirements adequately. Figure 2b shows the estimated trajectories of Gd ions in the FePt film at this energy. The damage calculation for this energy yielded a large value of 650 displacements per implanted atom, inducing a high density of vacancies in the film samples.

Four different implantations with Gd concentrations of 1, 2, 3, and 5 at. % were conducted at an incident angle of 7° in order to avoid channelling effects. The calculated fluences as well as the compositions and thicknesses, obtained by RBS measurements, are summarized in Table I. The desired Gd concentrations were achieved within the range of accuracy of RBS. An interesting observation is that the relative Fe content is strongly decreased at higher exposure doses, which is due to the higher sputter yield of Fe compared to Pt during Gd implantation. The Fe and Pt concentrations as function of Gd content (or dose) are given in Fig. 3a. The variation of the film thickness is shown in Fig. 3b, revealing a substantial reduction of over 40% for the highest exposure dose.

To evaluate the amount of damage to the $L1_0$ ordering caused by the implantation, XRD $\theta/2\theta$-scans of all samples were recorded (see Fig. 1b–e). A splitting of the FePt(002) peak into two peaks, especially for the highest Gd concentration, as shown in Fig. 1e, can be observed. The stronger of the two peaks at a lower angle belongs to the disordered $A1$ phase. The weaker (002) peak indicates the remaining $L1_0$ phase. The (001) peak that only exists for the $L1_0$ phase has strongly decreased in intensity when compared

**TABLE I**. Composition and thickness of as-prepared and Gd-implanted FePt films prepared by using different exposure doses $\Phi_{Gd}$. The values were extracted from RBS.

| $\Phi_{Gd}$ ($10^{15}$ atoms/cm$^2$) | Fe (at. %) | Pt (at. %) | Gd (at. %) | Thickness (nm) (from XRD) |
|---|---|---|---|---|
| 0 | 52 | 48 | 0 | 20.1 (19.9) |
| 1.47 | 51 | 48 | 1 | 17.7 (18.0) |
| 2.94 | 49 | 49 | 2 | 15.9 (15.1) |
| 4.41 | 46 | 51 | 3 | 14.1 (13.9) |
| 7.35 | 44 | 51 | 5 | 14.0 (11.3) |

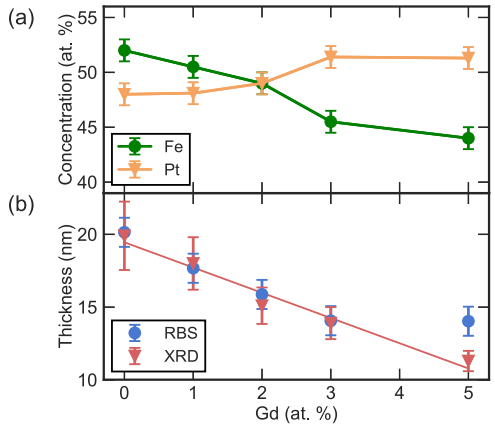


**FIG. 3**. (a) Relative Fe and Pt concentrations and (b) total film thickness as a function of Gd content according to RBS and XRD results.

to before implantation (see Fig. 1a). Even the smallest exposure dose destroyed the $L1_0$ ordering except for a small amount. As the remaining fraction of $L1_0$ phase seems to be equally present in all samples, the region in which the ordering could prevail must be at the film/substrate interface, as this region is barely affected by Gd ions (see Fig. 2).

Another observation that can be made is that the position of the $A1$ FePt(002) peak shifts towards lower angles for higher implantation doses, as shown in more detail in Fig. 1f. Due to the fact that the samples have slightly different sizes, the absolute measured intensities of the different samples cannot be compared to one another in a meaningful way and were therefore normalized to their maximum. The shift of the peak position in angular space corresponds to an increase in lattice spacing from $c$ = 3.818 Å for 1 at.% to $c$ = 3.855 Å for 5 at.% Gd. This behaviour is mainly a result of the $A1$ FePt phase getting richer in Pt due to the stronger resputter effect of Fe compared to Pt.

The decrease in film thickness for higher exposure doses manifests itself in the evident broadening of the diffraction peaks (see Fig. 1f). According to the Scherrer equation, the peak's half-width is inversely correlated to its coherent scattering length. The thicknesses extracted from XRD data as well as the thicknesses obtained from RBS measurements are shown in Fig. 3b, which are in good agreement except for the highest exposure dose. The XRD results appear more reasonable, as they imply a linear decrease in film thickness as the exposure dose increases and are therefore used in the following for calculating the film volume needed to determine the magnetization of the implanted samples.

To characterize the change in magnetic properties after implantation, in-plane and out-of-plane $M$-$H$ hysteresis loops were measured (see Fig. 4b–e). From the measurements, it becomes apparent

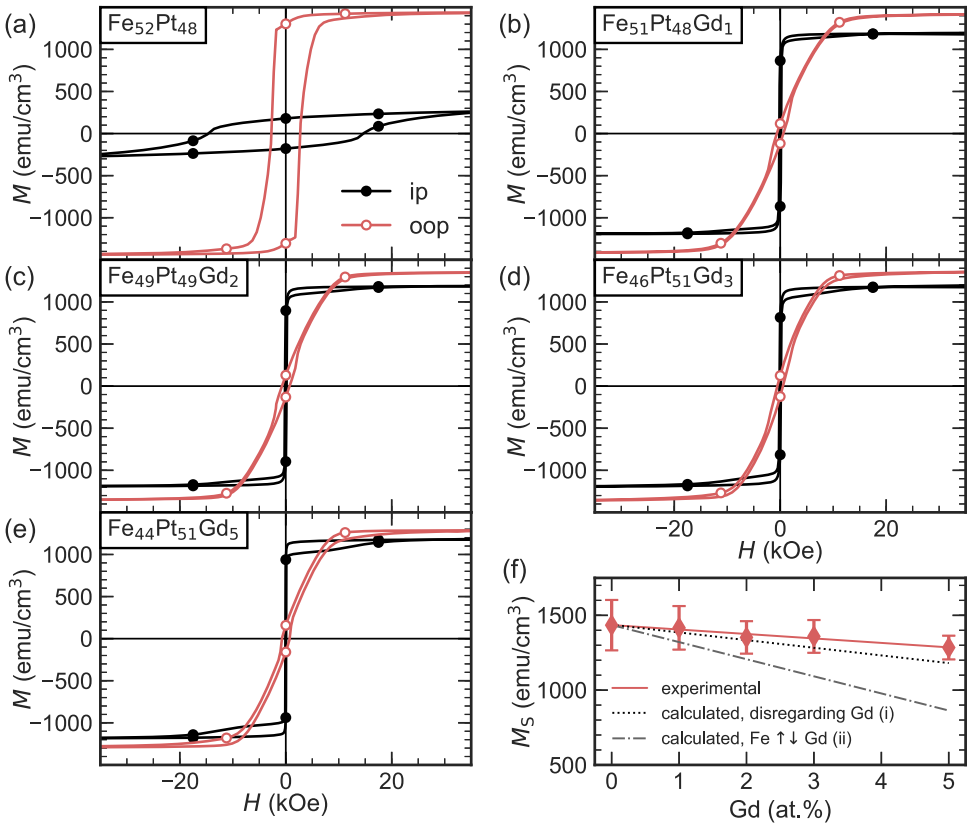


**FIG. 4**. $M$-$H$ hysteresis loops of (a) as-prepared $L1_0$ FePt and (b-e) after Gd implantation. (f) Comparison of measured and calculated $M_S$ values as a function of Gd concentration considering two cases: (i) only Fe moments contribute to the magnetization and (ii) Gd magnetic moments are coupled antiparallel to Fe.

that the out-of-plane $M_S$ seems to be larger than in-plane. This is due to an inherent error arising from the SQUID's pickup-geometry.[26] The loops reveal two distinct parts of reversal. A rather sharp switching at low fields in the range of tens of Oe and a reversal of magnetization at higher fields of up to 20 kOe. This observation is consistent with the conclusions drawn from the structural analysis, where two layers were suggested; a dominant $A1$ phase with an in-plane easy axis and a small $L1_0$ ordered region at the film/substrate interface exhibiting an easy axis out-of-plane. The chemically disordered $A1$ phase shows no magnetocrystalline anisotropy, therefore, the in-plane direction is now the preferred magnetic easy axis, due to magnetic shape anisotropy. We analyzed the evolution of $M_S$ in order to see some indication of magnetic coupling between Fe and Gd, which might be strongly antiferromagnetic, as observed in Fe-Gd alloys.[27,28] However, as shown in Fig. 4f, we found only a slight decrease in $M_S$ with Gd content, which is much lower than expected for antiferromagnetic coupling between Gd and Fe, assuming a Gd moment of 7.6 $\mu_B$.[29] Thus, the reduction is simply given by the reduced Fe content after implantation while Gd is considered to be in a paramagnetic state. Please note that $M$-$H$ loops taken at lower temperatures down to 50 K revealed the same behaviour.

In order to restore the desired $L1_0$ ordering, the samples were thermally post-annealed at 800 °C for one hour inside a tube furnace. The process was conducted in low pressure Ar atmosphere to prevent reactions with oxygen. The XRD $\theta/2\theta$-scan of the post-annealed $Fe_{51}Pt_{48}Gd_1$ sample is compared with the implanted sample shown in Fig. 5a and b, respectively. However, no transformation to the $L1_0$ structure could be observed. Even the previously measured $A1$ FePt(002) peak completely disappeared. Instead, a pure fcc Pt phase formed, which manifests itself in the occurence of the Pt(002) peak at around 46°. A striking feature of this peak compared to the previously measured FePt peaks is its small full width at half maximum. The coherent scattering length corresponding to this value is about 40 nm. Therefore, the Pt phase most likely appears in form of islands. The total lack of Fe-related peaks can be explained by oxidation of Fe in the sample by residual $O_2$ inside the Ar gas during annealing. We believe that it is thermodynamically distributed throughout the sample due to the high density of vacancies and structural defects introduced by Gd implantation. An XPS study determined the type of iron oxide to be $Fe_2O_3$ (not shown). In this regard, a systematic study on the oxidation of FePt nanoparticles was reported by C. Liu *et al.*[30] In their series of experiments, the change in structure after annealing in an oxygen rich atmosphere at different temperatures was investigated. Samples annealed at 700 °C exhibited no FePt compounds but consisted solely of pure Pt and $Fe_2O_3$, which is consistent with our observation.

The surface morphology of the post-annealed $Fe_{51}Pt_{48}Gd_1$ film was examined by AFM and SEM imaging. AFM measurements reveal a grainy film structures with a roughness $R_q$ of about 16 nm (see Fig. 6a), while SEM images show, in addition, separated regions of brighter and darker areas (see Fig. 6b, c). At eight selected spots, marked in Fig. 6c, AES was measured to gain insight on the local chemical composition at each spot. The measured Auger signal (Fig. 6d) shows a high Pt and low Fe and O concentration at bright areas, while darker regions show only Fe and O, suggesting a local phase separation between elementary Pt and iron oxide.

The change in magnetic properties induced by the post-annealing process were captured by another series of in-plane and out-of-plane $M$-$H$ hysteresis loops, one of which is compared to an implanted sample, as shown in Fig. 5c and d, respectively. The magnetization is still calculated assuming the same volume as before annealing. However, this is not necessarily the case, as the volume has changed as a result of the phase formation of Pt and $Fe_2O_3$. Both of these effects increase the overall volume as both Pt and any iron oxide exhibit a lower density than FePt.[3,31] The magnetization values given for the post-annealed sample are therefore not to be taken literally but are upper estimates of the actual magnetization.

The general shape of the measured $M$-$H$ loops strongly differs from any of the previously measured loops as the magnetization loops hardly show an opening at the centre. The coercivity has decreased by a factor of 20 and is now in the order of tens of Oe, as visible in the inset of Fig. 5d. Even though, the measured magnetization value, as mentioned previously, is an upper estimate, a striking decrease by about a factor of five is still noticeable when compared to before annealing, characteristic for weakly ferromagnetic $Fe_2O_3$.[32]

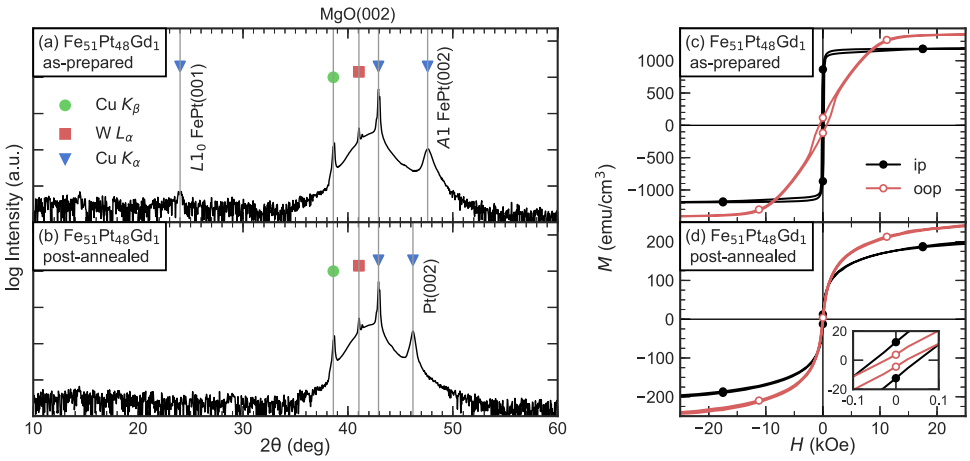


**FIG. 5.** XRD $\theta/2\theta$-scans of (a) Gd-implanted FePt and (b) after post-annealing. Corresponding $M$-$H$ hysteresis loops are shown in (c, d).

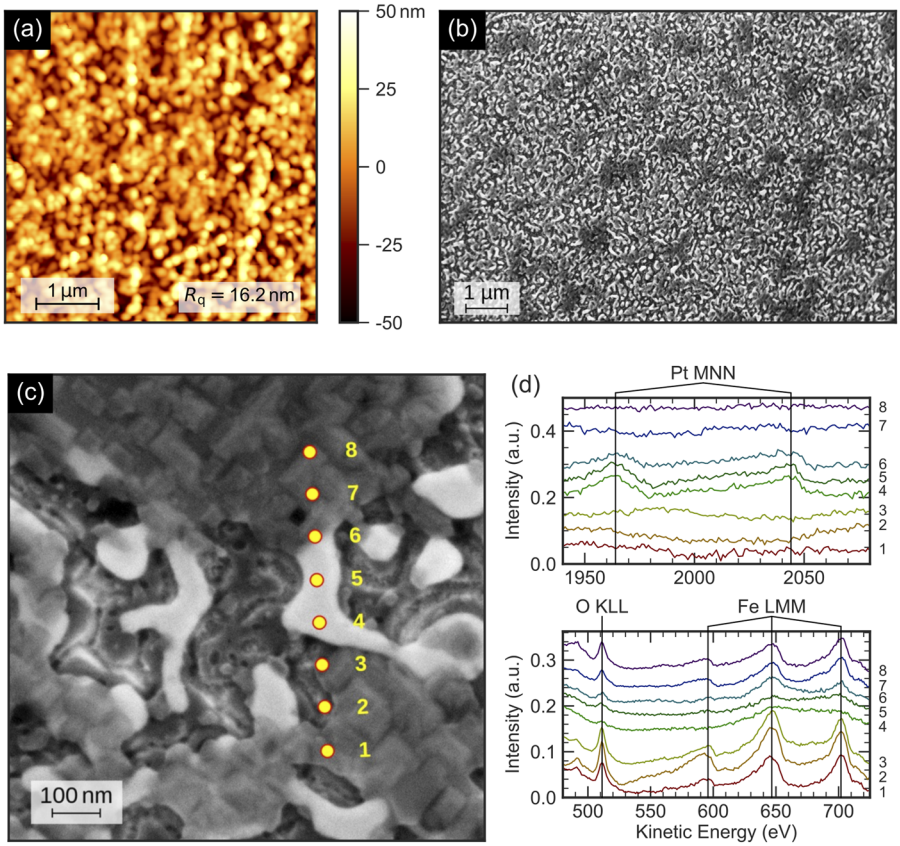


**FIG. 6**. (a) AFM image and (b, c) SEM image of the post-annealed $Fe_{51}Pt_{48}Gd_1$ sample. Marked spots in (c) indicate measurement points of AES analysis with the extracted spectra presented in (d). Bright areas show high Pt and low Fe and O content, whereas the darker regions reveal only iron oxide.

## IV. CONCLUSIONS

$L1_0$ ordered $Fe_{52}Pt_{48}$ films with a thickness of 20 nm and strong perpendicular magnetic anisotropy were sputter-deposited on MgO(001) at 800 °C. Four different Gd concentrations were then implanted at 30 keV to make up 1, 2, 3, and 5 at. % of Gd. The thickness of the film decreased continuously as more and more material was resputtered. During the implantation process, a stronger resputtering effect of Fe could be observed compared to Pt, decreasing the relative Fe/Pt ratio the more Gd was implanted. The $L1_0$ order was destroyed almost entirely by the process leaving behind only a thin ordered layer at the film/substrate interface. The magnetic easy axis turned in-plane and the high coercivity previously measured had disappeared. The continuous loss of Fe in the FePt alloy after implantation resulted in a decrease in $M_S$, without any signature of magnetic coupling between Fe and Gd. Thus, Gd is expected to be in a paramagnetic state. In an attempt to restore the $L1_0$ ordering by post-annealing at 800 °C in a low pressure Ar atmosphere, the material transformed to pure Pt and weakly ferromagnetic $Fe_2O_3$, faciliated by the presence of a high density of vacancies induced by the implantation process.

## ACKNOWLEDGMENTS

We would like to thank W. Brückner for assisting in Gd implantation, W. Reiber for RBS measurements, and Dr. M. Bauer for performing XPS measurements. This work was financially supported by the Deutsche Forschungsgemeinschaft (DFG, project number AL-618/31-1).

## REFERENCES

[1] R. F. C. Farrow, D. Weller, R. F. Marks, M. F. Toney, A. Cebollada, and G. R. Harp, J. Appl. Phys. **79**, 5967 (1996).
[2] A. Hotta, T. Ono, M. Hatayama, K. Tsumura, N. Kikuchi, S. Okamoto, O. Kitakami, and T. Shimatsu, J. Appl. Phys. **115**, 17B712 (2014).
[3] J. Lyubina, B. Rellinghaus, O. Gutfleisch, and M. Albrecht, in *Handbook of Magnetic Materials*, Vol. 19, edited by K. H. J. Buschow (Elsevier, 2011), pp. 291–395.
[4] D. Weller, O. Mosendz, G. Parker, S. Pisana, and T. S. Santos, Phys. Status Solidi A **210**, 1245 (2013).
[5] D. Weller, G. Parker, M. Oleksandr, A. Lyberatos, D. Mitin, N. Y. Safonova, and M. Albrecht, J. Vac. S. Technol. B **34**, 060801 (2016).
[6] D. Suess and T. Schrefl, Appl. Phys. Lett. **102**, 162405 (2013).
[7] M. T. Kief and R. H. Victora, MRS Bull. **43**, 87–92 (2018).
[8] K. Hono, Y. Takahashi, G. Ju, J.-U. Thiele, A. Ajan, X. Yang, R. Ruiz, and L. Wan, MRS Bull. **43**, 93–99 (2018).
[9] T. Ono, H. Nakata, T. Moriya, N. Kikuchi, S. Okamoto, O. Kitakami, and T. Shimatsu, AIP Adv. **6**, 056011 (2016).
[10] C. Brombacher, H. Schletter, M. Daniel, P. Matthes, N. Jöhrmann, M. Maret, D. Makarov, M. Hietschold, and M. Albrecht, J. Appl. Phys. **112**, 073912 (2012).
[11] M. Maret, C. Brombacher, P. Matthes, D. Makarov, N. Boudet, and M. Albrecht, Phys. Rev. B **86**, 024204 (2012).

[12]D. B. Xu, J. S. Chen, T. J. Zhou, and G. M. Chow, J. Appl. Phys. **109**, 07B747 (2011).
[13]J. Park, Y.-K. Hong, S.-G. Kim, L. Gao, and J.-U. Thiele, J. Appl. Phys. **117**, 053911 (2015).
[14]K. Kang, Z. G. Zhang, C. Papusoi, and T. Suzuki, Appl. Phys. Lett. **82**, 3284 (2003).
[15]M. L. Yan, Y. F. Xu, X. Z. Li, and D. J. Sellmyer, J. Appl. Phys. **97**, 10H309 (2005).
[16]B. S. D. C. S. Varaprasad, Y. K. Takahashi, J. Wang, T. Ina, T. Nakamura, W. Ueno, K. Nitta, T. Uruga, and K. Hono, Appl. Phys. Lett. **104**, 222403 (2014).
[17]D. B. Xu, C. J. Sun, J. S. Chen, S. M. Heald, B. Sanyal, R. A. Rosenberg, T. J. Zhou, and G. M. Chow, J. Phys. D: Appl. Phys. **48**, 255001 (2015).
[18]I. Radu, K. Vahaplar, C. Stamm, T. Kachel, N. Pontius, H. A. Dürr, T. A. Ostler, J. Barker, R. F. L. Evans, R. W. Chantrell, A. Tsukamoto, A. Itoh, A. Kirilyuk, T. Rasing, and A. V. Kimel, Nature **472**, 205 (2011).
[19]L. Le Guyader, S. El Moussaoui, M. Buzzi, R. V. Chopdekar, L. J. Heyderman, A. Tsukamoto, A. Itoh, A. Kirilyuk, T. Rasing, A. V. Kimel, and F. Nolting, Appl. Phys. Lett. **101**, 022410 (2012).
[20]T. A. Ostler, J. Barker, R. F. L. Evans, R. W. Chantrell, U. Atxitia, O. Chubykalo-Fesenko, S. El Moussaoui, L. Le Guyader, E. Mengotti, L. J. Heyderman, F. Nolting, A. Tsukamoto, A. Itoh, D. Afanasiev, B. A. Ivanov, A. M. Kalashnikova, K. Vahaplar, J. Mentink, A. Kirilyuk, T. Rasing, and A. V. Kimel, Nat. Commun. **3**, 666 (2012).
[21]A. Kirilyuk, A. V. Kimel, and T. Rasing, Rev. Mod. Phys. **82**, 2731 (2010).
[22]J. F. Ziegler, M. D. Ziegler, and J. P. Biersack, Nucl. Instrum. Methods Phys. Res **268**, 1818 (2010).
[23]B. W. Roberts, Acta Metall. **2**, 597 (1954).
[24]J.-U. Thiele, L. Folks, M. F. Toney, and D. K. Weller, J. Appl. Phys. **84**, 5686 (1998).
[25]T. Klemmer, D. Hoydick, H. Okumura, B. Zhang, and W. Soffa, Scr. Metall. Mater. **33**, 1793 (1995).
[26]M. Buchner, K. Höfler, B. Henne, V. Ney, and A. Ney, J. Appl. Phys. **124**, 161101 (2018).
[27]M. Mansmann and W. E. Wallace, J. Chem. Phys. **40**, 1167 (1964).
[28]P. Hansen, C. Clausen, G. Much, M. Rosenkranz, and K. Witter, J. Appl. Phys. **66**, 756 (1989).
[29]C. Vittoria, P. Lubitz, and V. Ritz, J. Appl. Phys. **49**, 4908 (1978).
[30]C. Liu, T. J. Klemmer, N. Shukla, X. Wu, D. Weller, M. Tanase, and D. Laughlin, J. Magn. Magn. Mater. **266**, 96 (2003).
[31]W. M. Haynes, *CRC Handbook of Chemistry and Physics*, 92nd ed. (CRC Press, 2011).
[32]A. Aharoni, E. H. Frei, and M. Schieber, Phys. Rev. **127**, 439 (1962).